Check for updates

Accepted Article

Dielectrophoretic manipulation of nanomaterials: a review

Linbo Liu, Ke Chen, Nan Xiang*, and Zhonghua Ni*

School of Mechanical Engineering, and Jiangsu Key Laboratory for Design and Manufacture of Micro-Nano Biomedical Instruments, Southeast University, Nanjing 211189, P. R. China.

E-mails: nan.xiang@seu.edu.cn, nzh2003@seu.edu.cn

Nan Xiang: http://orcid.org/0000-0001-9803-4783

Nanomaterials manipulation using dielectrophoresis (DEP) is one of the major research areas that could potentially benefit the micro/nano science for diverse applications, such as microfluidics, nanomachine and biosensor. The innovation and development of basic theories, methods or applications will have a huge impact on the entire related field. Specifically, for DEP manipulation of nanomaterials, improvements in comprehensive performance of accuracy, flexibility and scale could promote broader applications in micro/nano science. Therefore, to explore the directions for future research, this paper critically provides an overview on the fundamentals, recent progress, current challenges, and potential applications of DEP manipulation of nanomaterials. This review will also act as a guide and reference for researchers to explore promising applications in relevant research.

Color online: See article online to view Figs. 1–10 in color.

Keywords: Dielectrophoresis (DEP); Manipulation; Micro-/nano-electrodes; Nanomaterials

1. Introduction

Inspired by the macro creation of organisms in nature, scientists from multidisciplinary fields have explored various types of artificial manufacturing systems at nanoscale (10^{-9} m) based on nanotechnology [1–4]. Nanotechnology is a method to unfold the mysterious physics of nanoscale

Received: 08 14, 2018; Revised: 09 26, 2018; Accepted: 09 30, 2018

This article has been accepted for publication and undergone full peer review but has not been through the copyediting, typesetting, pagination and proofreading process, which may lead to differences between this version and the Version of Record. Please cite this article as doi: 10.1002/elps.201800342 .

This article is protected by copyright. All rights reserved.

Accepted Article

world. To build those nanoscale artificial systems, the building blocks and production tools are required. The basic building blocks used to create nanoscale products are a variety of nanomaterials, such as nanoparticle [5–7], nanowire [8, 9], graphene [10, 11] and so on [12, 13, 72‑77]. And the production tools at nanoscale are various types of field forces, such as electric field force [14], magnetic field force [15], hydrodynamic field force [16] and the force produced by the chemical reaction [17]. Dielectrophoresis (DEP) is one of these tools which utilizes the interaction between a non-uniform electric field and an induced dipole to manipulate various nanomaterials. And there is an increasing interest in implementing DEP technique for nanomaterial manipulation due to its advantages of label-free, noninvasive and low-cost [12]. Herein, what we call nanomaterial manipulation involves separating, trapping, rotating, propelling and assembling.

In recent years, the manipulation of nanomaterials using DEP technique has become an exponentially growing research focus [18–22]. However, there still remain some challenges on how to create arbitrary complex non-uniform electric field at nanoscale, and then achieving high precise, flexible and large-scale manipulation of nanomaterials. It is gratifying that scientists from multidisciplinary fields have made much subdivision of efforts in improving the accuracy, flexibility and scale of DEP manipulation of nanomaterials, which has laid a vital foundation for the researches of nanoscale manufacturing systems, drug delivery, precise nanosurgery and so on [23–31].

In this review, we critically provide an overview on the advances in DEP manipulation of nanomaterials over the latest five years. In the following sections, we firstly introduce the theory of DEP and the electrode configurations commonly used to manipulate nanomaterials. Then, we review the recent progress, current challenges, and potential applications of DEP manipulation of nanomaterials. Finally, we explore the outlook for recently developed DEP-based systems and the challenges that lie ahead.

2. Dielectrophoresis (DEP) theory for nanomaterials manipulation

When a polarizable nanomaterial is subjected to a non-uniform electric field, the force exerted on the nanomaterial causes it to move toward high or low field density regions; this behavior is known as dielectrophoresis [32]. Both DC and AC electric signals can be applied to electrodes to generate resultant forces across nanomaterials, thus leading to the DEP behavior. If the nanomaterial moves towards the electrode edge, the region of high electric field gradient, then the response is entitled positive DEP (pDEP). If the nanomaterial moves away from the electrode edge, then the response is

This article is protected by copyright. All rights reserved.

Accepted Article

entitled negative DEP (nDEP) [33]. The dielectrophoretic force exerted on a nanomaterial is dependent on: (1) nanomaterial's characteristics, such as its dielectric properties, size and shape, (2) the suspending medium's properties, such as conductivity and permittivity, and (3) the applied electric field, which produces the field gradient [26]. Simply put, the manipulation of nanomaterials in dielectrophoresis is based on the difference in polarizability between the nanomaterials and the surrounding medium. In order to get a better understanding of AC dielectrophoresis and DC dielectrophoresis, detailed introductions along with analytical expressions are given below.

2.1 Alternating current dielectrophoresis (AC-DEP)

2.1.1 Spheroid model (zero-dimensional nanomaterials)

The time averaged dielectrophoretic force on a spheroid is given as the following analytical expression [34]:

$$F_{DEP} = 2\pi r^3 \, \varepsilon_m \, Re(F_{CM}) \, \nabla|E^2| \quad (1)$$

The magnitude of the DEP force is linearly dependent on four variables: the particle volume (r^3), the permittivity of the medium (ε_m), the real part of the Clausius-Mossotti factor (F_{CM}), and the gradient of the squared external electric field ($\nabla|E^2|$), known as the field gradient factor. For an alternating electric field (AC-DEP), the root mean square value (| |) is used in the calculation.

F_{CM} is the Clausius-Mossotti factor that governs the frequency response and force direction in DEP manipulation. F_{CM} also is the value of dipole moment which represents the interaction between the nanomaterials and the medium (see Eq. (2a)):

$$F_{\mathrm{CM}} = \frac{\varepsilon_p^* - \varepsilon_m^*}{\varepsilon_p^* + 2\varepsilon_m^*} \quad (2a)$$

$$\varepsilon_p^* = \varepsilon_p - j\frac{\sigma_p}{\omega} \quad (2b)$$

$$\varepsilon_m^* = \varepsilon_m - j\frac{\sigma_m}{\omega} \quad (2c)$$

This article is protected by copyright. All rights reserved.

Accepted Article

where ε_p^* and ε_m^* are the complex permittivities of the particle and the medium, respectively. In Eqs. (2b) and (2c), ε and σ denote the electrical permittivity and conductivity, respectively, j is $\sqrt{-1}$, and ω is the angular frequency of the applied signal.

Equation (2a) indicates that, if $\varepsilon_p^* > \varepsilon_m^*$, particle is pulled toward high electric field density region, inducing the positive DEP (pDEP) phenomenon. If $\varepsilon_p^* < \varepsilon_m^*$, particle is pushed toward low electric field density region, inducing the negative DEP (nDEP) phenomenon.

Moreover, Eqs. (2-a, b, c) indicate that, if $\varepsilon_p^* = \varepsilon_m^*$, that is to say there is a frequency at which the $Re(F_{CM})$ becomes zero. This frequency is called as DEP crossover frequency (f_{cross}), which can be formulated for spheroid as [35]:

$$f_{\text{cross}} = \frac{1}{2\pi}\sqrt{\frac{(\sigma_m-\sigma_p)(\sigma_p+2\sigma_m)}{(\varepsilon_p-\varepsilon_m)(\varepsilon_p+2\varepsilon_m)}} \quad (3)$$

If two spheroids with similar size have different f_{cross}, different forms of manipulation (e.g., separation) based on dielectric property can be achieved with DEP. If f_{cross} values of nanomaterials are too close, they can be separated by size-based DEP, since DEP force is directly proportional to the cube of the radius of spheroid (see Eq. (1)).

For low frequency electric fields, the sign of the F_{CM} is determined by the electrical conductivities of the particle and the medium, see Eq. (4a). Whereas, for high frequency electric fields, the F_{CM} depends on the permittivity, see Eq. (4b) [28]:

$$\text{Low frequency:} \quad \lim_{\omega\to 0} Re(F_{CM}) = \frac{\sigma_p-\sigma_m}{\sigma_p+2\sigma_m} \quad (4a)$$

$$\text{High frequency:} \quad \lim_{\omega\to \infty} Re(F_{CM}) = \frac{\varepsilon_p-\varepsilon_m}{\varepsilon_p+2\varepsilon_m} \quad (4b)$$

Moreover, equation (4a) indicates that, for very low frequencies, if σ_p is much larger than σ_m, the F_{CM} will be at its maximum value of 1.0. In contrast, if σ_m is much larger than σ_p, then the F_{CM} will be at its minimum value of -0.5. These outcomes are also valid for very high field frequencies when permittivity is concerned in Eq. (4b) [35]. For spheroid, the F_{CM} varies between -0.5 and 1. As a

This article is protected by copyright. All rights reserved.

Accepted Article

result, the manipulation force on the nanomaterial under pDEP is generally higher than the force on the nanomaterial under nDEP.

In AC-DEP condition, the use of a high-frequency (>100 kHz) AC field has some advantages: (1) the electrothermal effects can be reduced, (2) electrochemical reactions, such as those producing gas (i.e., bubble generation) can be reduced and (3) no electrophoretic movement is observed due to the cell membrane being statically charged.

In concentrated suspensions, interparticle interactions become dominant when high gradient AC fields are applied. Hence, concentrated suspensions restrain the electric field strength for DEP applications [36].

2.1.2 High aspect-ratio oblate spheroid model (one, two-dimensional nanomaterials)

The Clausius-Mossotti factor for a high aspect-ratio oblate spheroid (one, two-dimensional nanomaterials) can be calculated as [37]:

$$F_{\mathrm{CM}}^{*} = \frac{\varepsilon_p^{*} - \varepsilon_m^{*}}{\varepsilon_m^{*}} \quad (5)$$

where $\varepsilon_{\mathrm{p}}^{*}$ and $\varepsilon_{\mathrm{m}}^{*}$ are the complex permittivies of the particle and fluid medium, respectively. The formulas of the complex permittivity refer to Eqs. (2-b, c).

Moreover, for other complicated nanomaterials, the effect of a multi-layered spheroid can be numerically determined by using an effective volume calculation for iterative layers. Models for elliptical particles (prolate and oblate geometries) contain an axis depolarization factor and have been used to represent spheroid such as bacteria [38].

A major factor in the effectiveness of the DEP force is the size of a particle; as the volume decreases, the force will also decrease. However, for extremely small nanomaterials such as DNA fragments, viruses, or cellular organelles, effective separation and trapping may cease below a certain size. At this limit, Brownian motion and random thermal drift will overcome any induced DEP force. An equation for the limit has been previously calculated by Hughes [39] for opposing electrodes with a fixed trap width or electrode gap (Δd).

$$r > \sqrt[3]{\frac{10KT}{\pi\varepsilon_m \, Re(F_{CM}) \, \nabla|E^2| \, \Delta d}} \quad (6)$$

This article is protected by copyright. All rights reserved.

Accepted Article

where K is Boltzmann's constant and T is the temperature.

2.2 Direct current dielectrophoresis (DC-DEP)

Direct current dielectrophoresis is a novel technique employing insulating objects or hurdles within the channel to create spatial field non-uniformities. It is also known as insulator-based dielectrophoresis (iDEP) or electrodeless dielectrophoresis (eDEP) or contactless dielectrophoresis (cDEP), owing to the fact that the electrodes are placed far outside the channel in the inlet and outlet ports.

Neglecting the frequency component for strict DC-DEP, the F_{CM} in Eq. (2a) is modified to Eq. (4a) [40].

$$F_{\mathrm{CM-DC}} = \frac{\sigma_p - \sigma_m}{\sigma_p + 2\sigma_m} \tag{7}$$

When the dimension of the material being manipulated is nanoscale, the manipulation of these nanoscale materials would be more affected by van der Waals force, electrostatic force and electrothermal force. However, when the distance between the material and the microelectrode is within the control radius and larger than 10 nanometers, the DEP force dominates. This control radius is the region where the DEP force (decaying exponentially in the far field) is larger than the other resistance force. So the simplification Eq. (7) could substituted into Eq. (1), yielding

$$F_{DEP} = 2\pi r^3 \varepsilon_m \frac{\sigma_p - \sigma_m}{\sigma_p + 2\sigma_m} \nabla \left| E_{DC}^2 \right| \tag{8}$$

where E_{DC} is the magnitude of the applied DC electric field.

DC-DEP techniques are advantageous compared to the classical AC-DEP manipulation. The advantages of using such insulating obstacles are enormous [26]: (1) electrochemical reactions are removed, (2) fabrication process is simpler and more stable because no embedded metal components are required, (3) the electrothermal effects can be reduced remarkably, (4) the samples are less affected by fouling, (5) devices are chemically inert and robust, (6) high manipulation efficiency of sensitive biological particles.

This article is protected by copyright. All rights reserved.

Accepted Article

However, electric field magnitude is inversely proportional to the gap between electrodes which is often in the order of centimeters in DC-DEP. Thus, if DEP manipulation device is performed under purely DC fields or <100 kHz AC fields, it often requires very high voltages to create a suitable electric field gradient for DEP manipulation, which in the meantime raises the risk of electric shock during operation [41].

2.3 (AC+DC)-DEP

Another novel manipulation technique is the combination of AC-DEP and DC-DEP which uses both AC and DC fields in the insulating obstacle geometry to achieve manipulation [42]. By using both AC and DC signals, high voltage DC signal can be reduced and replaced by the low frequency AC signal in the order of <100 kHz, thus reducing the potential problems of Joule heating and sample degradation [43]. Meanwhile, a larger manipulation area could be achieved and the fabrication process becomes simpler and more stable, owing to the fact that the electrodes could be placed outside the channel. The force associated with this form of DEP is a function of the ratio of both the AC and DC voltage, as defined by Zhang et al. [30]. Besides, some groups have accomplished outstanding achievements in DEP manipulation of nanomaterials by applying (AC+DC)-DEP, as discussed in part four.

2.4 Fluid force

2.4.1 Pressure-driven flows

It is obvious that fluid flows can be generated by applying hydrostatic pressure differences on the device. The most well-known example of such pressure-induced flow is the parabolic Hagen-Poiseuille profile in a straight channel [44]. Even in general channel designs with nontrivial structures (posts, constrictions, etc.), the main characteristics of pressure-driven flows are small flow velocities close to the device boundaries and high velocities in the middle of the fluidic channel.

The F_{flow} is the drag force for an isolated cylinder in laminar flows parallel to the axis of symmetry (the wall effect is neglected). The formula of F_{flow} is given as [45]:

$$F_{\text{flow}} = \frac{4\pi\mu Ua}{\ln(2a/b)-0.72} \quad (9)$$

This article is protected by copyright. All rights reserved.

Accepted Article

where μ is the viscosity of the fluid; U is the fluid velocity; a and b are the length and radius of the cylinder, respectively. From Eq. (9), it is found that the F_{flow} is proportional to velocity U which achieves the maximum at the channel centerline.

All of these formulas reveal that the F_{DEP} decays exponentially with increasing distance of nanomaterials away from the electrodes while the F_{flow} increases with increasing distance of nanomaterials away from the channel wall.

2.4.2 Electrothermal and electroosmotic flow

Except for generated by applying hydrostatic pressure, fluid flows can also induced from electric field gradients. Electric fields act on the nanomaterial suspension when there are gradients in the fluid charge density, which can pronouncedly impact the forces on nanomaterial. Electric-field-induced fluid flows are subdivided into two categories: electrothermal flow (ETF) and electroosmotic flow.

The applied electric field causing electric current flow in the solution and then Joule heating. Joule heating of the fluid induces permittivity and conductivity gradients, thus creating electrothermal force on the fluid. Afterwards, nanomaterials in the solution are subjected to motion by the imposed drag force from the electrothermal flow of the fluid [46, 47].

Another electric-field-induced fluid flow is electroosmotic flow. Electroosmosis is caused by the interaction of an electric field with free charges in the electric double layer and has its origin in the Coulomb force. Charges in the diffuse layer migrate in the vicinity of an interface due to the applied electric field and generate a drag flow in the fluid. If the electric field is nonuniform, an AC signal induces analogous behavior on metallic surfaces [46, 47]. In this force system, Brownian motion has been shown to be less of an impediment to the dielectrophoretic movement of nanomaterials [47]. The above electrophoresis theory provides the theoretical basis and tool for analyzing the forces and movement behavior of nanomaterials (nanoparticles, nanowires, etc.) in the following quoted articles.

3. Micro/nano-electrodes for nanomaterials manipulation

Dielectrophoretic manipulation, such as assembling, sorting, trapping, and electro-rotation, can be accomplished by applying different electrode patterns and electric signals (voltage, phase and frequency) [48]. Several years ago, non-uniform electric fields were produced using traditional electrodes, such as metal needles, wires, rods, and sheets. Electric field gradient is inversely

This article is protected by copyright. All rights reserved.

Accepted Article

proportional to the distance between electrodes [41]. To induce electric field gradients appropriate for required voltage levels, on the order of tens of volts, the gap between the electrodes must be optimized to the size of the nanomaterials intended to be manipulated. With the development of micro-fabrication techniques, it possible to fabricate precise micro/nano-electrodes to produce the needed specific field gradients [49].

The advantages in employing micro/nano-electrode are obvious. Firstly, the miniaturization substantially reduces the electrode decay and Joule heating effects, thus retaining the viability of suspension. And then, the dielectrophoretic force hinges on the gradient of the square of the electric field, and direct dimensional analysis has substantiated the substantial rise in dielectrophoretic force achieved with micro/nano-sized electrodes. So the dielectrophoretic force exerted on the nanomaterials vastly increases [26].

3.1 Internal electrodes

In recent decades, the vast majority of research works of nanomaterials manipulation performed on DEP has been done using internal electrodes. Internal electrodes are implant inside the microchannel producing non-uniform electric field directly and coming into contact with the nanomaterials and the suspending medium. There are a variety of materials that have been used in DEP applications but platinum and gold remain the best options given their proven good electrochemical stability and biocompatibility. Indium tin oxide (ITO), a sort of transparent conductor when applied in thin layers, is also democratic to fabricate microelectrodes following techniques similar to those applied to metals. The main potential imperfection of applying metal electrodes are electrolysis at high frequencies and fouling. The net aftereffect of these matters can be gas generation or dissolution of the electrodes, which might potentially damnify the nanomaterials being manipulated.

A huge diversity of electrode pattern designs have been applied by different research groups. There are some popular configurations applied to achieve DEP effects using an AC field, such as interdigitated microelectrodes [50, 51], multiphase electrodes [52], trapezoidal electrode array, checker board arrangement, and pyramidal arrangement [53]. The interdigitated electrode array is the most commonly used electrode pattern applied to achieve non-uniform electric field as it is easy to model and creates large arrays. The interdigitated electrode array comprises two sets of electrode arrays, with one of the sets designated as the ground [48]. Castellated electrodes are similar to interdigitated electrodes but they comprise square-wave-shaped electrodes. Those electrodes are positioned parallel to each other, and regions of field maxima and minima are produced [30]. Specially, there was a kind

This article is protected by copyright. All rights reserved.

Accepted Article

of leadless dot matrix electrodes pattern (internal electrodes), which could achieves continuous-area manipulation of nanomaterials without electric field interference from the leads [54].

3.2 External electrodes

Secondary common method of producing non-uniform electric field is the usage of external electrodes which is placed outside the channel of DEP chip. It is also known as electrodeless dielectrophoresis (eDEP) or insulator-based dielectrophoresis (iDEP) or contactless dielectrophoresis (cDEP). Instead of producing non-uniform electric field directly, the external electrodes are producing an relatively large area of uniform electric field, and then shape-designed insulating hurdle or obstacle in the microchannel is utilized to split the uniform electric field into the required non-uniform electric field [42]. The main advantage of applying external electrodes is that the electrodes are not fabricated along with the DEP device. This advantage to a large extent reduces the complexity and costs of the fabrication. Meanwhile, the problem of Joule heating is largely eased and there will be no bubbles generated from electrolytic reaction inside the channels.

The number and shape of these insulating hurdles can be designed according to the required non-uniform electric field, and meanwhile the microchannel itself can be shaped into any needed geometry. Several common geometries were explored including saw tooth channel [55], spiral [56], oil droplet [57], triangle [58], a serpentine microchannel [59, 60], and a rectangle [58, 61, 62].

A required complicated non-uniform electric field is created as the electric field lines diverge around the insulating hurdles. Owing to the insulating hurdles, a region of high electric field density is created within the narrow channel regions produced by the hurdles. The nanomaterials are driven by fluid flow through these narrow regions, while the field gradient shape aids in nanomaterials motion. Since dielectrophoretic forces drive the nanomaterials away from or toward the high electric field density, the nanomaterials experience a repulsive or attractive force as they flow around the corner of the hurdles, thus promoting nanomaterials motion according to its polarizability.

4. Dielectrophoretic manipulation of nanomaterials

This article is protected by copyright. All rights reserved.

Accepted Article

The main components of nanomaterial manipulation are manipulation methods (DEP) and manipulated objects (nanomaterials). In this section, there are four parts divided according to the morphological properties of the manipulated nanomaterials (Fig. 1): (1) zero-dimensional nanomaterials (nanoparticle, quantum dot etc.); (2) one-dimensional nanomaterials (nanowire, nanotube, nanorod, nanomotor etc.); (3) two-dimensional nanomaterials (graphene etc.); and (4) other nanomaterials (DNA, viruses, vesicles, supramoly, molecules, bacteria etc.). These nanomaterials almost have unique properties such as, physical property (e.g. high surface-to-volume ratio), mechanical property (e.g. outstanding robustness), electrical property (e.g. high carrier mobility) and versatile chemistry. And then, the three primary criteria for judging the ability of DEP manipulation of nanomaterials are discussed respectively: (1) accuracy; (2) flexibility; (3) scale.

In summary, the main challenge of putting forward the research in DEP manipulation of nanomaterials is how to create arbitrary complex non-uniform electric field in the nano-scale, and then achieving the high precise, flexible and large-scale manipulation of nanomaterials. Table 1 contains the key information of DEP manipulation collected from the articles we discussed below divided according to the morphological properties of the nanomaterials.

4.1 Zero-dimensional nanomaterials (nanoparticle, quantum dots etc.)

4.1.1 Nanoparticle

Nanoparticles are bulk materials that are three dimensional at the nanometer scale. In recent years, nanoparticles have been widely implemented for nanoscience applications [90-117]. Thus, effective and efficient nanoparticle manipulation are significant for advancement in these fields. Tanaka et al. (Fig. 2A) [82] achieved accurate DEP manipulation of the single nanoparticle passing through a solid-state pore. In their experiments, a trap field was created by applying AC electric signals between electrodes embedded in a low-aspect-ratio micro-pore. Besides, accurate DEP manipulation technique was applied to assemble multifarious nano-sensors which had excellent performance in sensitivity, repeatability and stability [76, 77, 81, 84]. Besides, extensive researches had been accomplished about continuous accurate separation of nanoparticles based on DEP technique [81].

Knigge et al. (Fig. 2B) [78] achieved the large-scale temporary or permanent immobilisation of polystyrene (PS) nanoparticles on vertical nano-electrodes by dielectrophoresis-based technique. The electrodes had diameters of 50 nm or 500 nm, respectively, and were fabricated in arrays of several thousand electrodes, allowing huge amount of experiments simultaneously. Moreover, Gallego et al. (Fig. 2C) [118] achieved large-scale pyroelectric manipulation and patterning of nanoparticles in

This article is protected by copyright. All rights reserved.

Accepted Article

lithium niobate opposite domain structures. They for the first time used the specific ferroelectric domain structure of periodic opposite domain lithium niobate (ODLN) crystals for structured nanoparticle manipulation. In particular, the surface charge density created by a temperature change in this pyroelectric material was the fountainhead of the trapping forces: electrophoretic on charged ones and dielectrophoretic on neutral particles.

The year ensuing, Rozynek et al. (Fig. 3A) [5] achieved large-scale formation of printable colloidal and granular chains through dielectrophoresis and capillary effects. The chains were automatically stabilized by liquid bridges formed between adjacent nanoparticles, without the need for special particle functionalization or continuous energy input. This study advances the scale of nanoparticle assembly from micrometer scale to centimeter scale.

Outstanding performance in the comprehensive ability of accuracy, flexibility and scale was achieved in the researches of Cihan Yilmaz et al. (Fig. 3B) [83]. They demonstrated that colloidal nanoparticles could be manipulated and simultaneously accumulated into three-dimensional metallic nanostructures with complex geometries such as nanorings, nanoboxes and nanopillars with feature sizes of 25 nm in less than one minute by applying externally electric field. The systematic study of the DEP manipulation of nanoparticles has laid a vital foundation for the applications of single cell analysis, targeted drug delivery and precise nanosurgery. Besides, increasing number of relevant and promising applications is to be developed by multidiscipline scientists.

4.1.2 Quantum dots (QDs)

Quantum dot is a kind of special nanoparticle (nanoscale semiconductors) and it can emit a specific frequency of light when applying a certain electric field or light. Accurate assembly of arrays of QDs-nanowire hybrid for location deterministic biochemical detection was achieved by Liu et al. (Fig. 4A) [87]. QDs (diameter < 10 nm) were precisely positioned on the tips of the pre-assembled Au nanowires. The mechanisms of manipulation were quantitatively understood as the cooperative effects of alternating current electroosmosis (ACEO) and dielectrophoresis due to AC electric fields.

Flexible manipulation of single QDs and polystyrene nanoparticles at a gold nanostructure by applying the AC-dielectrophoretic force was achieved by Kim et al. (Fig. 4B) [86]. Manipulation in three degrees of freedom (end-facet, side, and position-selective manipulation) was actualized in gold nanostructures between microelectrodes.

This article is protected by copyright. All rights reserved.

Accepted Article

Nasti et al. (Fig. 4C) [85] has achieved large-scale, complex and reversible manipulation of CdSe quantum dots driven by pyroelectric-dielectrophoresis. They investigated experimentally the dynamic behaviors of CdSe QDs by time-lapse fluorescence microscopy imaging. Specially, the QDs for visualization, manipulation and measurement were immersed in polydimethylsiloxane (PDMS) fluid. Their research opened the pathway for designing a switchable and reversible device allowing two different final QDs-patterned states.

4.2 One-dimensional nanomaterials (nanowire, nanotube, nanorod, nanomotor etc.)

In the aspect of accuracy of nanomaterials manipulation, Leiterer et al. (Fig. 5A) [71] achieved accurate manipulation of single silicon nanowire and sufficient contact between nanowire and two pre-patterned electrodes by applying DEP-based technique. In the same year, high precise manipulation and actuation of arrays of nanowire were achieved by Kim et al. (Fig. 5B) [70]. In this work, they reported innovative mechanisms for accurate manipulation and actuation of nanowire arrays that could synchronously oscillate between two pre-designed positions for over 4000 cycles. The actuation mechanisms and manipulation were based on dielectrophoresis (DEP)-based technique and unique magnetic interactions between perpendicular magnetic anisotropy (PMA) with nanoentities.

In the aspect of flexibility of nanomaterials manipulation, Liu et al. (Fig. 6A) [54] presented a novel ‘leadless’ dielectrophoresis chip with dot matrix electrodes (LDME-DEP chip) fabricated by stacking three different functional layers. The LDME-DEP chip excels mainly in two aspects: (1) they for the first time applied the technique of separating the lead and the electrode pattern into two different layers to manipulate nanowires, which achieved continuous-area manipulation of nanowires without interference from the lead; (2) the use of dot matrix electrodes made the manipulation more flexible. In the same year, Wang et al. (Fig. 6B) [65] achieved flexible assembly of Ag nanowire arrays with arbitrarily angle on an independent, removable polyethylene terephthalate (PET) film by rotating the reusable ITO electrodes. The PET film was placed on the reusable ITO electrodes, and a sinusoidal AC electric signal was applied to the electrodes to induce DEP force for nanowire assembly upon the flexible film. And then, Boehm et al. (Fig. 6C) [64] achieved reconfigurable positioning of vertically-oriented nanowires around topographical features through dielectrophoretic and electrohydrodynamic forces which were manipulated through frequency and voltage variation. Nanowires were assembled in water solution between two parallel plane electrodes, where the bottom plane electrode was patterned with cylindrical photoresist posts.

This article is protected by copyright. All rights reserved.

Accepted Article

In the aspect of scale of nanomaterials manipulation, conventional DEP manipulation of nanomaterials using electric fields has been restricted to small scale structures. Bornhoeft et al. (Fig. 7A) [72] broke this limitation by applying the Tesla coil's antenna to create a gradient high-voltage force field that projected into free space. This was an upgraded form of DEP, which they called Teslaphoretic (TEP). They showed that carbon nanowires placed within the TEP field polarized and self-assembled into wires at remote distances (>30 cm). Thus, the scale of the manipulation of nanomaterials span from the nanoscale to the macroscale was achieved through this technique. Besides, another work of large scale manipulation of nanomaterials was achieved by Venkatesh et al. (Fig. 7B) [68]. They achieved directed assembly of ultrathin Au nanowires over large area fingertip pointing shaped electrodes using AC DEP. On the basis of the electric signal (voltage and frequency), the ultrathin Au nanowires either at the sides of or align between the electrodes. Moreover, numerous research works about fabricating various high performance surface emitting LEDs has been accomplished based on large-scale assembly of nanomaterials [74, 75].

Outstanding performance in the comprehensive ability of those three indicators (accuracy, flexibility, scale) was achieved in the researches of Guo et al. (Fig. 8A) [9]. They reported a precise and controllable method in manipulating nanomotors by strategically applying three-dimensional electric fields. With the high controllability, the nanomotors demonstrated versatility in capturing, transporting, and releasing of cargos to pre-designated destination. Under the combination of DC and AC electric fields, nanomotors could effectively change their speeds instantly by the DC electric fields and accurately aligned by the AC electric fields. Within the three-dimensional orthogonal micro-electrode sets, the in-plane delivering of nanomotors could be fleetly turned on and off, and these nanomotors could also move in the perpendicular direction. In the same year, Yu et al. (Fig. 8B) [63] achieved the simultaneous Automated characterization, manipulation, and assembly of nanowires (ACMAN) with selectable electrical conductivities into nanodevices by applying an integrated DEP-based method. These multiple individual nanowires could be selected according to their electrical characteristics and precisely positioned at different locations in a low-conductivity liquid to form functional nanodevices with desired electrical properties. In addition, there are numerous other relevant excellent researches based on DEP manipulation of one-dimensional nanomaterials, which are not be discussed in detail here [119–144].

4.3 Two-dimensional nanomaterials (graphene etc.)

Graphene is a two-dimensional, schistose nanomaterial with high specific surface area, excellent chemical and physical properties. Thus, efficient and effective graphene manipulation is crucial for

This article is protected by copyright. All rights reserved.

Accepted Article

advancement in nano-science and technology. Oh et al. (Fig. 9A) [145] achieved high-precise and selective positioning of high-quality graphene sheets on a transparent and flexible polyethylene substrate by applying dielectrophoresis- based technique. In the same year, Park et al. (Fig. 9B) [146] achieved high accurate and large scale assembly of graphene under a non-uniform electric field. Graphene flakes were aligned precisely with the pre-defined Ti/Au electrodes on SiO2/Si substrate. A remarkable increase in conductivity and carrier mobility was observed after vacuum annealing at 100 °C.

Wang et al. (Fig. 9C) [89] achieved large-scale assembly of graphene oxide (GO) nanostructures mixed with platinum (Pt) nanoparticles between the parallel finger electrodes. The Pt-modified GO nanostructures were well positioned between a pair of pre-patterned Ti/Au electrodes by applying the DEP technique with the optimized parameters. Two year later, Hong et al. (Fig. 9D) [10] demonstrated electric-field-induced isotropic- nematic or biphase-nematic phase separation applying dielectrophoretic condensation of GO particles in a dispersion medium. Large-scale assembly of GO using dielectrophoresis had advantage that the spatial shape of phase separation could be arbitrarily tailored through electrode design, and the GO was well aligned. This work corroborated that DEP was a powerful tool to manipulate and assemble GO in wet dispersions. Besides, some other relevant researches based on DEP manipulation of two-dimensional nanomaterials are not be discussed in detail here [147–166].

4.4 Other nanomaterials (DNA, viruses, vesicles, supramoly, molecules, bacteria etc.)

Kopperger et al. (Fig. 10A) [12] created a 55-nm–by–55-nm DNA-based molecular platform with an integrated robotic arm (length of 25 nm), which could be lengthened to more than 400 nm and actuated with DEP-based technique. Specially, computer-controlled switching of this integrated robotic arm between arbitrary positions on the platform could be realized within milliseconds. Moreover, the arm could be used for electrically driven transport of nanoparticles or molecules over tens of nanometers.

Schäfer et al. (Fig. 10B) [167] achieved accurate assembly of bovine serum albumin (BSA) molecules on arrays of metallic nanocones by dielectrophoresis. The gold nanocones are integrated into a microfluidic channel and used as nanoelectrodes. By applying an AC voltage, BSA molecules near the nanocones in the channel would be captured by DEP. After assembly of the BSA molecules, the plasmonic nanostructures can be directly demonstrated by optical read-out techniques (Fig. 10B-d).

This article is protected by copyright. All rights reserved.

Accepted Article

Another accurate DEP manipulation of nanomaterials was achieved by Barik et al. (Fig. 10C) [13]. They excogitated that atomically sharp edges of single-layer graphene could create singular electrical field gradients for manipulating nanomaterials through dielectrophoresis-based technique. They found that graphene-edge dielectrophoresis could generate 10 times higher gradient forces as compared to metal electrodes. Thus, they achieved near-100% nanoparticle accurate positioned at an extremely voltage (0.45 V) with nanodiamonds, nanobeads, and DNA within seconds through graphene-edge dielectrophoresis. Graphene-edge dielectrophoresis puts forward the physical limit of gradient-force based manipulating by generating atomically sharp tweezers. Besides, some other researches accomplished based on DEP manipulation of nanomaterials, such as MoS_2 nanosensors fabricated by dielectrophoretic assembly for ultrasensitive and rapid sensing of volatile organic compounds [168].

5. Conclusion and outlook

The research in DEP manipulation of nanomaterials opens a door of putting forward macro science and technology into nanoscale world. There are three main criteria for judging the ability of DEP manipulation of nanomaterials which are also challenges we need to put efforts into: (1) accuracy; (2) flexibility; (3) scale. In summary, the main challenge of putting forward the research in dielectrophoresis manipulation of nanomaterials is how to create arbitrary complex non-uniform electric field in the nanoscale, and then improving the comprehensive performance in the ability of those three indicators, achieving high precise, flexible and large-scale manipulation of nanomaterials.

Until now, scientists from multidisciplinary fields have explored and developed numerous excellent DEP manipulation systems. However, due to the drawback that dielectrophoretic mechanism is not compatible with high-ionic-strength biological fluids, in vivo applications based on current nanomaterials manipulation and assembly face significant challenges. Future research efforts might be looking into the possibility of solving this problem. Moreover, a possible step-forward in improving the comprehensive performance of those three indicators is the usage of AC+DC, Teslaphoretic (TEP, an upgraded form of DEP), three-dimensional electrodes and dot matrix electrode pattern, thus achieving the high precise, flexible and large-scale manipulation of nanomaterials. In particular, the manipulation scale span from the nanoscale to the macroscale (>30 cm) was achieved through using TEP. In addition, the usage of three-dimensional electrodes enables the three-dimensional manipulation of nanomaterials. Thorough consideration of the aforementioned suggestions might pave the way for more attention and development in DEP manipulation of nanomaterials.

The developments in the research of DEP manipulation of nanomaterials are likely to have profound impact upon diverse applications, such as nanodevice manufacture, directed drug delivery,

This article is protected by copyright. All rights reserved.

Accepted Article

and precise nanosurgery. Given the enormous interests in this cutting-edge research field, we anticipate inexhaustible innovative ideas and useful applications in the future. With such careful attention to requirements and key challenges, along with developments and innovations, DEP manipulation of nanomaterials is expected to have tremendous impact on diverse applications, providing infinite opportunities limited only by one's imagination. These gradually accumulated developments will eventually revolutionize nano-science and technology, leading to significant improvements in the quality of our life and facilitating the realization of the glorious future vision.

Conflicts of interest

The authors have declared no conflict of interest.

Acknowledgements

This research work is supported by the National Natural Science Foundation of China (51875103, 51505082, 81727801, and 51775111), the Natural Science Foundation of Jiangsu Province (BK20150606), the Fundamental Research Funds for the Central Universities (2242017K41031), the Six Talent Peaks Project of Jiangsu Province (SWYY-005), and the Jiangsu Graduate Innovative Research Program (KYCX17_0062).

6 Notes and references

[1] Morrow, T. J., Li, M., Kim, J., Mayer, T. S., Keating, C. D., *Science*, 2009, 323, 352-352.

[2] Freer, E. M., Grachev, O., Duan, X., Martin, S., Stumbo, D. P., *Nat. Nanotechnol.*, 2010, 5, 525-530.

[3] Aïzel, K., Agache, V., Pudda, C., Bottausci, F., Fraisseix, C., Bruniaux, J., Fouillet, Y., *Lab Chip*, 2013, 13, 4476-4485.

[4] Laocharoensuk, R., Palaniappan, K., Smith, N. A., Dickerson, R. M., Werder, D. J., Baldwin, J. K., Hollingsworth, J. A., *Nat. Nanotechnol.*, 2013, 8, 660-666.

[5] Rozynek, Z., Han, M., Dutka, F., Garstecki, P., Józefczak, A., Luijten, E., *Nat. Commun.*, 2017, 8, 15255.

[6] Zhao, K., Peng, R., Li, D., *Nanoscale*, 2016, 8, 18945-18955.

[7] Dies, H., Raveendran, J., Escobedo, C., Docoslis, A., *Nanoscale*, 2017, 9, 7847-7857.

[8] Yang, T., Liu, L., Deng, Y., Guo, Z., Zhang, G., Ge, Z., Chen, H., *Adv. Mater.*, 2017, 29, 9.

This article is protected by copyright. All rights reserved.

Accepted Article

[9] Guo, J., Gallegos, J. J., Tom, A. R., Fan, D., *ACS nano*, 2018, 12, 1179-1187.

[10] Hong, S. H., Shen, T. Z., Lee, B., Song, J. K., *Part. Part. Syst. Charact.*, 2017, 34, 1600344.

[11] Wang, T., Huang, D., Yang, Z., Xu, S., He, G., Li, X., Zhang, L., *Nano-Micro Lett.*, 2016, 8, 95-119.

[12] Kopperger, E., List, J., Madhira, S., Rothfischer, F., Lamb, D. C., Simmel, F. C., *Science*, 2018, 359, 296-301.

[13] Barik, A., Zhang, Y., Grassi, R., Nadappuram, B. P., Edel, J. B., Low, T., Oh, S. H., *Nat. Commun.*, 2017, 8, 1867.

[14] Chang, Y. C., Wägli, P., Paeder, V., Homsy, A., Hvozdara, L., van der Wal, P., Herzig, H. P., *Lab Chip*, 2012, 12, 3020-3023.

[15] Zhang, L., Petit, T., Lu, Y., Kratochvil, B. E., Peyer, K. E., Pei, R., Nelson, B. J., *ACS Nano*, 2010, 4, 6228-6234.

[16] Wang, W., Castro, L. A., Hoyos, M., Mallouk, T. E., *ACS Nano*, 2012, 6, 6122-6132.

[17] Gibbs, J. G., Zhao, Y. P., *Appl. Phys. Lett.*, 2009, 94, 163104.

[18] Lim, J., Majetich, S. A., *Nano Today*, 2013, 8, 98-113.

[19] Lü, M., Li, J., Yang, X., Zhang, C., Yang, J., Hu, H., Wang, X., *Chin. Sci. Bull.*, 2013, 58, 2698-2710.

[20] Toda, K., Furue, R., Hayami, S., *Anal. Chim. Acta*, 2015, 878, 43-53.

[21] Wang, J. and Gao, W., *ACS Nano*, 2012, 6, 5745-5751.

[22] Pethig, R., *Adv. Drug Delivery Rev.*, 2013, 65, 1589-1599.

[23] Li, J., Rozen, I., Wang, J., *ACS Nano*, 2016, 10, 5619-5634.

[24] Sun, D. M., Liu, C., Ren, W. C., Cheng, H. M., *Small*, 2013, 9, 1188-1205.

[25] Salafi, T., Zeming, K. K., Zhang, Y., *Lab Chip*, 2017, 17, 11-33.

[26] Adekanmbi, E. O., Srivastava, S. K., *Lab Chip*, 2016, 16, 2148-2167.

[27] Varghese, S. S., Lonkar, S., Singh, K. K., Swaminathan, S., Abdala, A., *Sens. Actuators, B*, 2015, 218, 160-183.

[28] Demircan, Y., Özgür, E., Külah, H., *Electrophoresis*, 2013, 34, 1008-1027.

[29] Martinez‐Duarte, R., *Electrophoresis*, 2012, 33, 3110-3132.

[30] Zhang, C., Khoshmanesh, K., Mitchell, A., Kalantar-zadeh, K., *Anal. Bioanal. Chem.*, 2010, 396, 401-420.

This article is protected by copyright. All rights reserved.

Accepted Article

[31] Tu, Y., Peng, F., Wilson, D. A., *Adv. Mater.*, 2017, 29, 1701970.

[32] Nakano, A., Ros, A., *Electrophoresis*, 2013, 34, 1085-1096.

[33] Abd Rahman, N., Ibrahim, F., Yafouz, B., *Sensors*, 2017, 17, 449.

[34] Pethig, R., *Biomicrofluidics*, 2010, 4, 022811.

[35] White, C. M., Holland, L. A., Famouri, P., *Electrophoresis*, 2010, 31, 2664-2671.

[36] Kumar, A., Qiu, Z., Acrivos, A., Khusid, B., Jacqmin, D., *Phys. Rev. E*, 2004, 69, 021402.

[37] Freer, E. M., Grachev, O., Duan, X., Martin, S., Stumbo, D. P., *Nat. Nanotechnol.*, 2010, 5, 525.

[38] Fernádez-Morales, F. H., Duarte, J. E., Samitier-Martí, J., *An. Acad. Bras. Cienc.*, 2008, 80, 627-638.

[39] Hughes, M. P., *Nanoelectromechanics in engineering and biology*, CRC press, 2002.

[40] Keshavamurthy, S. S., Leonard, K. M., Burgess, S. C., Minerick, A. R., *NSTI-Nanotech, Boston, MA*, 2008, 1-5.

[41] Martinez‐Duarte, R., Renaud, P., Madou, M. J., *Electrophoresis*, 2011, 32, 2385-2392.

[42] Srivastava, S. K., Gencoglu, A., Minerick, A. R., *Anal. Bioanal. Chem.*, 2011, 399, 301-321.

[43] Zhu, J. Xuan, X., *Electrophoresis*, 2009, 30, 2668-2675.

[44] Bruus, H., *Theoretical microfluidics*, Oxford: Oxford university press, 2008.

[45] Happel, J., Brenner, H., *Low Reynolds number hydrodynamics: with special applications to particulate media*, Springer Science Business Media, 2012.

[46] Morgan, H. and Green, N. G., *AC electrokinetics*, Research Studies Press, 2003.

[47] Ramos, A., Morgan, H., Green, N. G., Castellanos, A., *J. Phys. D: Appl. Phys.*, 1998, 31, 2338.

[48] Kirby, B. J., *Micro-and nanoscale fluid mechanics: transport in microfluidic devices*, Cambridge university press, 2010.

[49] Hughes, M. P., *Electrophoresis*, 2002, 23, 2569-2582.

[50] Pethig, R., Huang, Y., Wang, X. B., Burt, J. P., *J. Phys. D: Appl. Phys.*, 1992, 25, 881.

[51] Yang, J., Huang, Y., Wang, X. B., Becker, F. F., Gascoyne, P. R., *Anal. Chem.*, 1999, 71, 911-918.

[52] Huang, Y. and Pethig, R., *Meas. Sci. Technol.*, 1991, 2, 1142.

[53] Pham, P., Texier, I., Larrea, A. S., Blanc, R., Revol-Cavalier, F., Grateau, H., Perraut, F., *J. Electrost.*, 2007, 65, 511-520.

This article is protected by copyright. All rights reserved.

Accepted Article

[54] Liu, L., Chen, K., Huang, D., Wang, X., Xiang, N., Ni, Z., *Nanotechnol.*, 2017, 28, 285302.

[55] Chen, K. P., Pacheco, J. R., Hayes, M. A., Staton, S. J., *Electrophoresis*, 2009, 30, 1441-1448.

[56] Zhu, J., Tzeng, T. R. J., Xuan, X., *Electrophoresis*, 2010, 31, 1382-1388.

[57] Barbulovic-Nad, I., Xuan, X., Lee, J. S., Li, D., *Lab Chip*, 2006, 6, 274-279.

[58] Kang, Y., Li, D., Kalams, S. A., Eid, J. E., *Biomed. Microdevices*, 2008, 10, 243-249.

[59] Zhang, L., Bastemeijer, J., Mollinger, J., Bossche, A., *NEMS 2008. 3rd IEEE International Conference on. IEEE*, 2008, 864-868.

[60] Zhu, J., Xuan, X., *J. Colloid Interface Sci.*, 2009, 340, 285-290.

[61] Srivastava, S. K., Daggolu, P. R., Burgess, S. C., Minerick, A. R., *Electrophoresis*, 2008, 29, 5033-5046.

[62] Kang, K. H., Kang, Y., Xuan, X., Li, D., *Electrophoresis*, 2006, 27, 694-702.

[63] Yu, K., Yi, J. and Shan, J. W., *Lab Chip*, 2018, 18, 1494-1503.

[64] Boehm, S. J., Lin, L., Brljak, N., Famularo, N. R., Mayer, T. S., Keating, C. D., *Langmuir*, 2017, 33, 10898-10906.

[65] Wang, X., Chen, K., Liu, L., Xiang, N., Ni, Z., *Nanotechnol.*, 2017, 29, 025301.

[66] Constantinou, M., Hoettges, K. F., Krylyuk, S., Katz, M. B., Davydov, A., Rigas, G. P., Shkunov, M, *Appl. Phys. Lett.*, 2017, 110, 133103.

[67] Constantinou, M., Rigas, G. P., Castro, F. A., Stolojan, V., Hoettges, K. F., Hughes, M. P., Shkunov, M., *ACS Nano*, 2016, 10, 4384-4394.

[68] Venkatesh, R., Kundu, S., Pradhan, A., Sai, T. P., Ghosh, A., Ravishankar, N., *Langmuir*, 2015, 31, 9246-9252.

[69] Chen, Y., Ding, X., Steven Lin, S. C., Yang, S., Huang, P. H., Nama, N., Gu, Y., *ACS Nano*, 2013, 7, 3306-3314.

[70] Kim, K., Zhu, F. Q., Fan, D., *ACS Nano*, 2013, 7, 3476-3483.

[71] Leiterer, C., Broenstrup, G., Jahr, N., Urban, M., Arnold, C., Christiansen, S., Fritzsche, W., *J. Nanopart. Res.*, 2013, 15, 1628.

[72] Bornhoeft, L. R., Castillo, A. C., Smalley, P. R., Kittrell, C., James, D. K., Brinson, B. E., Cherukuri, P.. *ACS Nano* 2016, 10, 4873-4881.

[73] Cao, Q., Han, S. J., Tulevski, G. S., *Nat. Commun.*, 2014, 5, 5071.

This article is protected by copyright. All rights reserved.

Accepted Article

[74] Eo, Y. J., Yoo, G. Y., Kang, H., Lee, Y. K., Kim, C. S., Oh, J. H., Do, Y. R., *ACS Appl. Mater. Interfaces*, 2017, 9, 37912-37920.

[75] Park, H. K., Yoon, S. W., Eo, Y. J., Chung, W. W., Yoo, G. Y., Oh, J. H., Do, Y. R., *Sci. Rep.*, 2016, 6, 28312.

[76] Ding, H., Shao, J., Ding, Y., Liu, W., Tian, H., Li, X., *ACS Appl. Mater. Interfaces*, 2015, 7, 12713-12718.

[77] Wang, J., Rathi, S., Singh, B., Lee, I., Maeng, S., Joh, H. I., Kim, G. H., *Sens. Actuators, B*, 2015, 220, 755-761.

[78] Knigge, X., Wenger, C., Bier, F. F., Hölzel, R., *J. Phys. D: Appl. Phys.*, 2018, 51, 065308.

[79] Zhou, P., Yu, H., Yang, W., Wen, Y., Wang, Z., Li, W. J., Liu, L., *ACS Appl. Mater. Interfaces*, 2017, 9, 16715-16724.

[80] Rathi, S., Kwak, Y., Jing, L., Yi, K. S., Baik, J. M., Kim, G. H., *Curr. Appl. Phys.*, 2017, 17, 351-357.

[81] Fu, K., Chen, S., Zhao, J., Willis, B. G., *ACS Sens.*, 2016, 1, 444-450.

[82] Tanaka, S., Tsutsui, M., Theodore, H., Yuhui, H., Arima, A., Tsuji, T., Kawai, T., *Sci. Rep.*, 2016, 6, 31670.

[83] Yilmaz, C., Cetin, A. E., Goutzamanidis, G., Huang, J., Somu, S., Altug, H., Busnaina, A., *ACS Nano*, 2014, 8, 4547-4558.

[84] Leiterer, C., Berg, S., Eskelinen, A. P., Csaki, A., Urban, M., Törmä, P., Fritzsche, W., *Sens. Actuators, B*, 2013, 176, 368-373.

[85] Nasti, G., Coppola, S., Olivieri, F., Vespini, V., Pagliarulo, V., Ferraro, P., *Langmuir*, 2018, 5, 2198-2204.

[86] Kim, J., Hwang, K. S., Lee, S., Park, J. H., Shin, H. J., *Nanoscale*, 2015, 7, 20277-20283.

[87] Liu, C., Kim, K., Fan, D. L., *Appl. Phys. Lett.*, 2014, 105, 083123.

[88] Peng, Y., Ye, J., Zheng, L., Zou, K., *RSC Adv.*, 2016, 6, 24880-24888.

[89] Wang, J., Rathi, S., Singh, B., Lee, I., Joh, H. I., Kim, G. H., *ACS Appl. Mater. Interfaces*, 2015, 7, 13768-13775.

[90] Ding, H., Liu, W., Shao, J., Ding, Y., Zhang, L., Niu, J., *Langmuir*, 2013, 29, 12093-12103.

[91] Chaurey, V., Rohani, A., Su, Y. H., Liao, K. T., Chou, C. F., Swami, N. S., *Electrophoresis*, 2013, 34, 1097-1104.

[92] Wood, N. R., Wolsiefer, A. I., Cohn, R. W., Williams, S. J., *Electrophoresis*, 2013, 34, 1922-1930.

This article is protected by copyright. All rights reserved.

Accepted Article

[93] Koiry, S. P., Celestin, M. E., Ratnadurai, R., Veerender, P., Krishnan, S., Aswal, D. K., Bhansali, S., *Electrophoresis*, 2013, 34, 1182-1188.

[94] Chuang, C. H., Wu, H. P., Huang, Y. W., Chen, C. H., *Biosens. Bioelectron.*, 2013, 48, 158-164.

[95] He, X., Hu, C., Guo, Q., Wang, K., Li, Y., Shangguan, J., *Biosens. Bioelectron.*, 2013, 42, 460-466.

[96] Hwang, Y., Sohn, H., Phan, A., Yaghi, O. M., Candler, R. N., *Nano Lett.*, 2013, 13, 5271-5276.

[97] Muñoz-Martínez, J. F., Elvira, I., Jubera, M., García-Cabañes, A., Ramiro, J. B., Arregui, C., Carrascosa, M., *Opt. Mater. Express*, 2015, 5, 1137-1146.

[98] Cheng, I. F., Chen, T. Y., Lu, R. J., Wu, H. W., *Nanoscale Res. Lett.*, 2014, 9, 324.

[99] Sano, N., Nakamura, T., Tamon, H., Suntornlohanakul, T., Poonjarernsilp, C., Charinpanitkul, T., *J. Appl. Phys.*, 2014, 115, 154302.

[100] Grilli, S., Coppola, S., Nasti, G., Vespini, V., Gentile, G., Ambrogi, V., Ferraro, P., *RSC Adv.*, 2014, 4, 2851-2857.

[101] Pesch, G. R., Du, F., Schwientek, U., Gehrmeyer, C., Maurer, A., Thöming, J., Baune, M., *Sep. Purif. Technol.*, 2014, 132, 728-735.

[102] McCanna, J. P., Sonnenberg, A., Heller, M. J., *J. Biophotonics*, 2014, 7, 863-873.

[103] Cherukulappurath, S., Lee, S. H., Campos, A., Haynes, C. L., Oh, S. H., *Chem. Mater.*, 2014, 26, 2445-2452.

[104] Jose, J., Kress, S., Barik, A., Otto, L. M., Shaver, J., Johnson, T. W., Oh, S. H., *ACS photonics*, 2014, 1, 464-470.

[105] Kim, G. H., Kwak, Y., Lee, I., Rathi, S., Baik, J. M., Yi, K. S., *ACS Appl. Mater. Interfaces*, 2014, 6, 14812-14818.

[106] Leiterer, C., Wünsche, E., Singh, P., Albert, J., Köhler, J. M., Deckert, V., Fritzsche, W., *Anal. Bioanal. Chem.*, 2016, 408, 3625-3631.

[107] Chiou, C. H., Chien, L. J., Kuo, J. N., *Applied Physics Express*, 2015, 8, 085201.

[108] Leiterer, C., Deckert‐Gaudig, T., Singh, P., Wirth, J., Deckert, V., Fritzsche, W., *Electrophoresis*, 2015, 36, 1142-1148.

[109] Bakewell, D. J., Bailey, J., Holmes, D., *Electrophoresis*, 2015, 36, 1443-1450.

[110] Nhan, V., *Lab Chip*, 2015, 15, 3056-3064.

[111] Liu, W., Wang, C., Ding, H., Shao, J., Ding, Y., *Appl. Surf. Sci.*, 2016, 370, 184-192.

[112] Dash, S., Mohanty, S., Pradhan, S., Mishra, B. K., *J. Taiwan Inst. Chem. Eng.*, 2016, 58, 39-48.

This article is protected by copyright. All rights reserved.

Accepted Article

[113] Zhong, X., Sun, Y., Kang, C., Wan, G., *Eur. J. Biomed. Res.*, 2017, 2, 7-11.

[114] Chai, Z., Yilmaz, C., Busnaina, A. A., Lissandrello, C. A., Carter, D. J., *Nanotechnol.*, 2017, 28, 475303.

[115] Almeida, G. B., Poppi, R. J., da Silva, J. A. F., *Analyst*, 2017, 142, 375-379.

[116] Huang, H., Ou‐Yang, H. D., *Electrophoresis*, 2017, 38, 1609-1616.

[117] Crivellari, F., Mavrogiannis, N., Gagnon, Z., *Sens. Actuators, B*, 2017, 240, 926-933.

[118] Gallego, A., García-Cabañes, A., Carrascosa, M., Arizmendi, L., *J. Phys. Chem. C*, 2015, 120, 731-736.

[119] Hwang, T. Y., Choi, Y., Song, Y., Eom, N. S. A., Kim, S., Cho, H. B., Choa, Y. H., *J. Mater. Chem. C*, 2018, 6, 972-979.

[120] Šutka, A., Joost, U., Järvekülg, M., Timusk, M., *Colloid Interface Sci. Commun.*, 2018, 22, 34-37.

[121] Cammi, D., Zimmermann, K., Gorny, R., Vogt, A., Dissinger, F., Gad, A., Waldvogel, S. R., *J. Phys. Chem. C*, 2018. 122, 1852-1859.

[122] Ho, H. H., Lin, C. L., Tsai, W. C., Hong, L. Z., Lyu, C. H., Hsu, H. F., *Nanoscale Res. Lett.*, 2018, 13, 21.

[123] Xing, Y., Dittrich, P. S., *Sensors*, 2018, 18, 134.

[124] Yu, N., Shi, Q., Nakajima, M., Wang, H., Yang, Z., Sun, L., Fukuda, T., *J. Micromech. Microeng.*, 2017, 27, 105007.

[125] dos Santos, M. V. P., Béron, F., Pirota, K. R., Diniz, J. A., Moshkalev, S., in *Nanowires-New Insights*, InTech, 2017.

[126] Rushi, A. D., Datta, K. P., Ghosh, P., Mulchandani, A., Shirsat, M. D., *Sens. Actuators, B*, 2018, 257, 389-397.

[127] Lin, Y. H., Lin, W. S., Wong, J. C., Hsu, W. C., Peng, Y. S., Chen, C. L., *Microchim. Acta*, 2017, 184, 2419-2428.

[128] Fan, H. H., Jin, C. C., Wang, Y., Hwang, H. L., Zhang, Y. F., *Ceram. Int.*, 2017, 43, 5875-5880.

[129] Tao, Q., Jiang, M., Li, G., *IEEE Transactions on Nanotechnol.*, 2014, 13, 517-526.

[130] Choi, K., Choi, W., Yu, C., Park, Y. T., *J. Nanomater.*, 2017.

[131] Núñez, C. G., Braña, A. F., López, N., Pau, J. L., García, B. J., 2017, 10353.

[132] Shao, F., Fan, J. D., Hernández-Ramírez, F., Fàbrega, C., Andreu, T., Cabot, A., Ali, S. Z., *Sens. Actuators, B*, 2016, 226, 110-117.

This article is protected by copyright. All rights reserved.

Accepted Article

[133] Sam, M., Moghimian, N., Bhiladvala, R. B., *Mater. Lett.*, 2016, 163, 205-208.

[134] Collet, M., Salomon, S., Klein, N. Y., Seichepine, F., Vieu, C., Nicu, L., Larrieu, G., *Adv. Mater.*, 2015, 27, 1268-1273.

[135] Palapati, N. K. R., Pomerantseva, E., Subramanian, A., *Nanoscale*, 2015, 7, 3109-3116.

[136] Kotsuki, K., Obata, S., Saiki, K., *Langmuir*, 2016, 32, 644-649.

[137] Pau, J. L., Waters, J., Rivera, E., Kim, S. M., Kung, P., *IEEE Electron Device Lett.*, 2015, 36, 814-816.

[138] Montemurro, D., Stornaiuolo, D., Massarotti, D., Ercolani, D., Sorba, L., Beltram, F., Roddaro, S., *Nanotechnol.*, 2015, 26, 385302.

[139] Galliker, P., Schneider, J., Poulikakos, D., *Appl. Phys. Lett.*, 2014, 104, 073105.

[140] Ramón‐Azcón, J., Ahadian, S., Estili, M., Liang, X., Ostrovidov, S., Kaji, H., Khademhosseini, A., *Adv. Mater.*, 2013, 25, 4028-4034.

[141] Puttaswamy, S. V., Lin, C. H., Sivashankar, S., Yang, Y. S., Liu, C. H., *Sens. Actuators, B*, 2013, 178, 547-554.

[142] García Marín, A., García Núñez, C., Ruiz, E., Piqueras, J., Pau, J. L., *Appl. Phys. Lett.*, 2013, 102, 232105.

[143] Núñez, C. G., Marín, A. G., Nanterne, P., Piqueras, J., Kung, P., Pau, J. L., *Nanotechnol.*, 2013, 24, 415702.

[144] Opoku, C., Hoettges, K. F., Hughes, M. P., Stolojan, V., Silva, S. R. P., Shkunov, M., *Nanotechnol.*, 2013, 24, 405203.

[145] Oh, S., Park, H., Jung, Y., Kim, J., Kim, J., Suk Oh, M., *J. Vac. Sci. Technol., B: Nanotechnol. Microelectron.: Mater., Process., Meas., Phenom.*, 2014, 32, 020602.

[146] Park, H., Oh, S., Kim, J., *ECS Solid State Lett.*, 2014, 3, M15-M17.

[147] Ahadian, S., Naito, U., Surya, V. J., Darvishi, S., Estili, M., Liang, X., Matsue, T., *Carbon*, 2017, 123, 460-470.

[148] Hasan, N., Zhang, W., Radadia, A. D., *Nanomater.*, 2017, 7, 339.

[149] Scalese, S., Baldo, S., D'Angelo, D., Filice, S., Bongiorno, C., Reitano, R., La Magna, A., *J. Appl. Phys.*, 2017, 121, 155105.

[150] Sihar, N., Dee, C. F., Mohamed, M. A., Yaw, T. T., Salleh, M. M., Majlis, B. Y., Abid, M. A. A. M., *Semiconductor Electronics (ICSE), 2016 IEEE International Conference on.* IEEE, 2016, 332-335.

This article is protected by copyright. All rights reserved.

Accepted Article

[151] Holovchenko, A., Dugay, J., Giménez‐Marqués, M., Torres‐Cavanillas, R., Coronado, E., van der Zant, H. S., *Adv. Mater.*, 2016, 28, 7228-7233.

[152] Fernandez, R. E., Sanghavi, B. J., Farmehini, V., Chávez, J. L., Hagen, J., Kelley-Loughnane, N., Swami, N. S., *Electrochem. Commun.*, 2016, 72, 144-147.

[153] Li, Y., Guan, Y., Liu, Y., Yin, J., Zhao, X., *Nanotechnol.*, 2016, 27, 195702.

[154] Sanghavi, B. J., Varhue, W., Rohani, A., Liao, K. T., Bazydlo, L. A., Chou, C. F., Swami, N. S., *Lab Chip*, 2015, 15, 4563-4570.

[155] Liu, S., Wang, Z., Zhang, Y., Zhang, C., Zhang, T., *Sens. Actuators, B*, 2015, 211, 318-324.

[156] Oikonomou, A., Clark, N., Heeg, S., Kretinin, A., Varey, S., Yu, G., Vijayaraghavan, A., *Phys. Status Solidi RRL*, 2015, 9, 539-543.

[157] Tungkavet, T., Seetapan, N., Pattavarakorn, D., Sirivat, A., *Polym.*, 2015, 70, 242-251.

[158] Gromova, Y., Alaferdov, A., Rackauskas, S., Ermakov, V., Orlova, A., Maslov, V., Fedorov, A., *J. Appl. Phys.*, 2015, 118, 104305.

[159] Latif, U., Dickert, F., *Sens.*, 2015, 15, 30504-30524.

[160] Ameri, S. K., Singh, P. K., Sonkusale, S., *Biosens. Bioelectron.*, 2014, 61, 625-630.

[161] Kybert, N. J., Han, G. H., Lerner, M. B., Dattoli, E. N., Esfandiar, A., Johnson, A. C., *Nano Res.*, 2014, 7, 95-103.

[162] Alaferdov, A. V., Gholamipour-Shirazi, A., Canesqui, M. A., Danilov, Y. A., Moshkalev, S. A., *Carbon*, 2014, 69, 525-535.

[163] Sanghavi, B. J., Varhue, W., Chávez, J. L., Chou, C. F., Swami, N. S., *Anal. Chem.*, 2014, 86, 4120-4125.

[164] Yuan, W., Shi, G., *J. Mater. Chem. A*, 2013, 1, 10078-10091.

[165] Li, Y. T., Qu, L. L., Li, D. W., Song, Q. X., Fathi, F., Long, Y. T., *Biosens. Bioelectron.*, 2013, 43, 94-100.

[166] Wang, J., Singh, B., Park, J. H., Rathi, S., Lee, I. Y., Maeng, S., Kim, G. H., *Sens. Actuators, B*, 2014, 194, 296-302.

[167] Schäfer, C., Kern, D. P., Fleischer, M.. *Lab Chip*, 2015, 15, 1066-1071.

[168] Wang, S. P., Wu, C. H., Hong, C. C., *SENSORS, 2015 IEEE*, 1-4.

This article is protected by copyright. All rights reserved.

Accepted Article

Table 1 Summary of Key Information in DEP Manipulation of Nanomaterials

Nanomaterials			Electrode		Electric Signals Applied		Comprehensive Performance (10-point System)			Group/ References
Type	Materials	Size (Diameter/ Length)	Type	Materials	Voltage	Frequency	Accuracy	Flexibility	Scale	
Nanowire	Silicon	——	Multiple combinations	Au	-50~50 Vpp	30 Hz~4 MHz	8	9	7	Yu et al. (2018) [63]
	Au	300 nm/ 2.5 μm	Parallel coplanar	ITO, Au	170, 330, 500 V/cm	5~50, 750 kHz, 10 MHz	7	7	8	Boehm et al. (2017) [64]
	Ag	100 nm/ 20~200 μm	Leadless dot matrix	ITO, Ag	0.1~2 Vpp	10 kHz, 1 MHz, 10 MHz	8	9	7	Liu et al. (2017) [54]
	Ag	100 nm/ 20~200 μm	Fingerlike electrodes	ITO	1~70 Vpp	10 kHz, 1 MHz, 10 MHz	7	8	9	Wang et al. (2017) [65]
	Silicon	75 nm/ 22 μm	Interdigitated finger	gold-plated copper	2.1~5 Vpp	1 kHz~ 20 MHz	7	6	8	Marios et al. (2017) [66]
	Silicon	30 nm/ <22 μm	Rectangular shaped	Au	5, 10, 15, 20 V	5 kHz~	7	6	8	Marios et al.

This article is protected by copyright. All rights reserved.

Accepted Article

						20 MHz				(2016) [67]
	Au	~2 nm/ 2.5 μm	Fingertip pointing	Au	2, 5, 10 Vpp	2, 10, 20 MHz	9	6	6	Venkatesh et al. (2015) [68]
	Ag	60 nm/ 40 μm	Standing surface acoustic waves	virtual electrodes	——	12.6~37 MHz	7	7	9	Chen et al. (2013) [69]
	Au/Ni/Au	150 nm/ 10 μm	Quadrupole	Au, Cr/Ni/Au	——	——	8	7	6	Kim et al. (2013) [70]
	Silicon	130 nm/ 10 μm	planar triangle-shaped	——	0.3, 5 V	1 MHz	7	7	6	Christian et al. (2013) [71]
Nanotube	Carbon	1, 25, 10, 85 μm/ 60 μm	Teslaphoresis	Tesla coil	1~10 V	2 MHz	6	6	10	Bornhoeft et al. (2016) [72]
	Carbon	200~500 nm / 21±6 nm	Parallel finger	Ti/Pd/Au	5 V	400 kHz	9	6	6	Cao et al. (2014) [73]
Nanorod	GaN/InGaN	50-200, 500 nm/ 2~3 μm	Interdigitated finger	Ti/Au	AC: 21 Vrms; DC: -21~+21 V	60 Hz	7	6	9	Eo et al. (2017) [74]
	InGaN/GaN	500 nm/ 2.5 μm	Interdigitated finger	Au	14, 17.5, 21 Vrms	950 kHz	7	6	9	Park et al. (2016) [75]
Nanomotor	Pt, Au, Ni, Ti, Cr,	250 nm/ 2~8 μm	Quadrupole	ITO, Au	AC:10~50 Vpp; DC:-1~	5 kHz~50MH	8	9	6	Guo et al.

This article is protected by copyright. All rights reserved.

Accepted Article

	Ag				+1V	z				(2018) [9]
Nanoparticle/ Nanowire	Au/ZnO	20 nm/ 200 nm, 4~5 μm	planar triangle-shaped	Al, Cr, Pd	3 V	10 kHz~ 1 MHz	8	6	6	Ding et al. (2015) [76]
Nanoparticle/ Graphene oxide	Pt	15 nm	Microgap	Au	5 V	500 kHz	8	6	7	Wang et al. (2015) [77]

Table 1 (*continued*)

Nanomaterials			**Electrode**		**Electric Signals Applied**	
Type	**Materials**	**Size (Diameter/ Length)**	**Type**	**Materials**	**Voltage**	**Frequency**
Nanoparticle	Polystyrene	1, 2 μm	Microporous array	ITO	1.7~13.7 Vrms	15 kHz
	Silica	100 nm, 15, 25, 55, 100, 200 μm	Needle-shaped	Al	100~600 V	20 kHz
	Ag	50 nm	Castellated	Cr, Au	1, 2.5 Vpp	1-100 Hz
	Polystyrene	200 nm	Pin shaped	ITO	5, 10 Vpp	10 kHz, 10 MHz
	Pd, Au	2~4 nm	Parallel finger	Ti/Au	1, 2, 3, 4 V	1 MHz
	Au	10 nm	Pin and plane	Pd, Ti	4 Vpp	1 MHz
	Polystyrene	780 nm	Micropore with four pins	Pt	0.1~10 V	2~10 MHz
	Au	<10 nm, >20 nm	Plane and microporous array	Cr/Au	12~20 Vpp	30~70 kHz
	Au	5, 15, 30, 60 nm	Microgap	Au	0.7~20 Vpp	1 kHz~1 MHz, 20MHz
Quantum	CdSe	3.4 nm	Dot matrix	Virtual	——	——

This article is protected by copyright. All rights reserved.

Accepted Article

dots				electrodes		
	_	20 nm	Microgap	Au	8 Vpp	1 MHz
	Semi-conductor	<10 nm	Microgap	Au	20 V	50 kHz~ 2 MHz
Graphene oxide	Carbon	550 nm	Stripe	ITO	0~20 V	10 kHz
	Carbon	100 nm	Triangle	Ti/Au	10 V	1 MHz
	Carbon	1 nm	Microgap	Ti/Au	2, 5, 10 Vpp	500 kHz
Molecules	DNA	4~55 nm	Robotic arm	DNA	——	0.1~25 Hz
	DNA	2 nm	Graphene electrodes	Cr/Au	0.45, 0.75,1.5, 2, 2.5, 3 V	100 kHz, 1~10 MHz

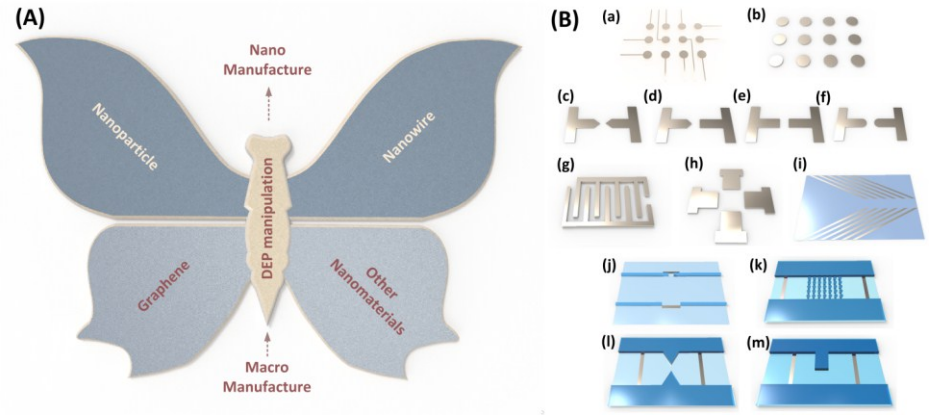

Fig. 1 (A) The research in DEP manipulation of nanomaterials (zero-dimensional, one-dimensional, two-dimensional and other nanomaterials) has laid vital foundation on putting forward macro science and technology into nanoscale world. The gradually accumulated developments in DEP manipulation of nanomaterials will eventually arouse *The Butterfly Effect* to revolutionize all the other nano-science and technology, leading to significant improvements in the quality of our life, and facilitating the realization of the glorious future vision. (B) Most commonly used microelectrodes are the combination or array of the smallest electrode elements in B-(a-m). Furthermore, these electrode units are divided according to the dimensions of the nanomaterials they are commonly used to manipulate. Internal electrodes: (a-b, i) zero-dimensional; (c-f) one-dimensional; (g-h) two-dimensional and other nanomaterials. External electrodes: (j-m) zero-dimensional.

This article is protected by copyright. All rights reserved.

Accepted Article

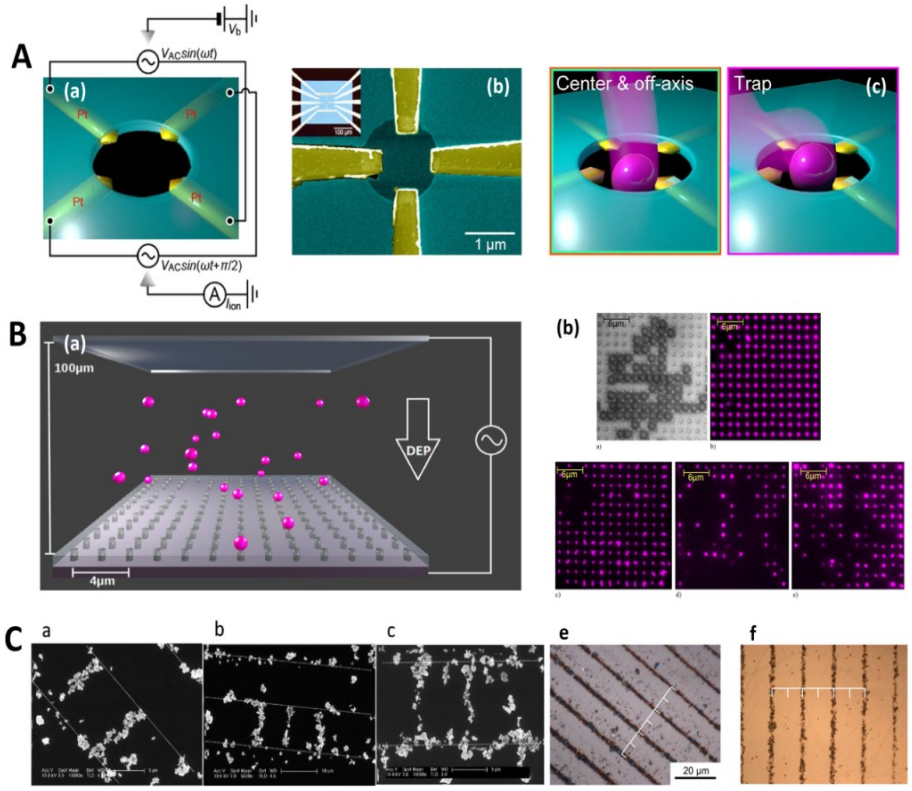

Fig. 2 (A): (a) Schematic illustrations of a four-electrode embedded micropore. (b) SEM image of a micropore consisting of a hole in a thick SiN membrane with four Pt electrodes arranged in a cross-wise configuration. (c) The schematic models for characteristic I_{ion} signals. (B): (a) Schematic illustration of the electrode configuration. (b) Micrographs of DEP immobilised nanoparticles. (C): (a-c) SEM images of trapped nanoparticles forming chains. (e, f) Micrographs of Ag nanoparticles trapped mainly on alternate domain walls

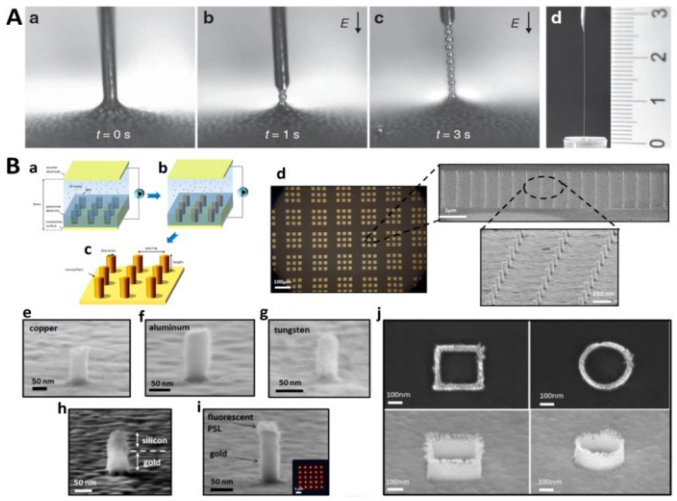

This article is protected by copyright. All rights reserved.

Fig. 3 (A): Experimental realization. (a-c) Pulling a conductive chain out of a container filled with a dispersion of Ag-coated hollow silica spheres in silicone oil. (d) A nearly 3-cm-long chain comprising hundreds of particles. (B): (a, b) NPs suspended in water solution are (a) assembled and (b) fused. (c) Removal of the patterned insulator film. (e-g) Fabricated nanopillars made of (e) copper, (f) aluminum, (g) tungsten, (h) gold and silicon, (i) gold and fluorescent PSL. (j) Top-down and high-angle SEM images of a 3-D nanobox and a nanoring.

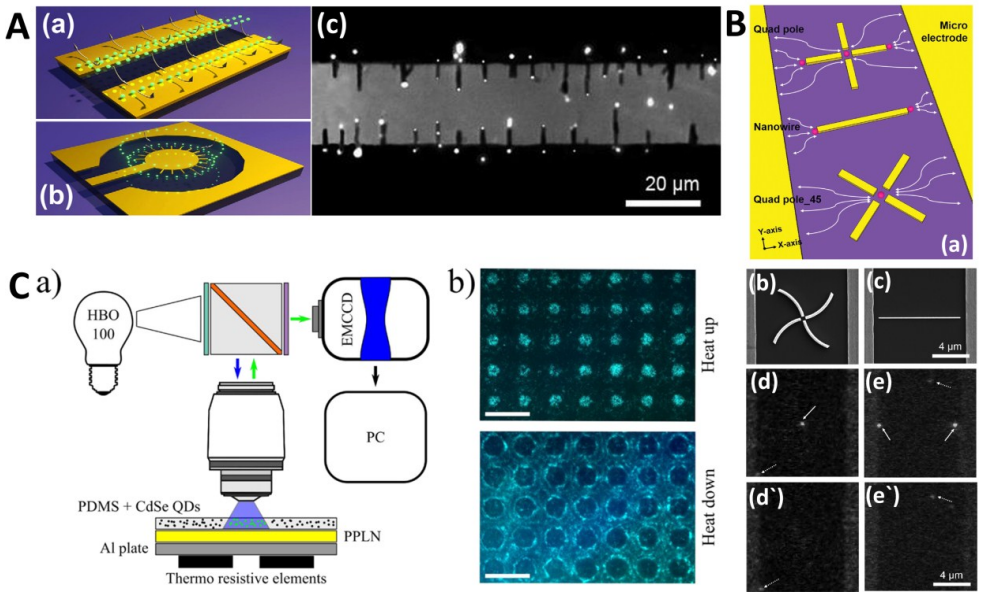

Fig. 4 (A): (a) Schematic diagram of ACEO flows for QDs manipulation. (b) Schematic diagram of manipulation QDs in the circular microelectrodes. (c). Quantum dots can be precisely positioned on the tips of arrays of nanowires. (B): (a) Schematic view of nanoparticle manipulation at metal nanostructures and the calculated electric field around nanostructures with the floating DEP force. (b-e') Manipulated single QD at Au nanostructures (C): Schematization of the optical setup used for the acquisition of the frame sequences (a) and two opposite QDs patterns achievable by the same periodically poled lithium niobate (PPLN) crystal after heating (top) and cooling (bottom) the crystal (b) (scale bar 200 µm)

Accepted Article

This article is protected by copyright. All rights reserved.

Accepted Article

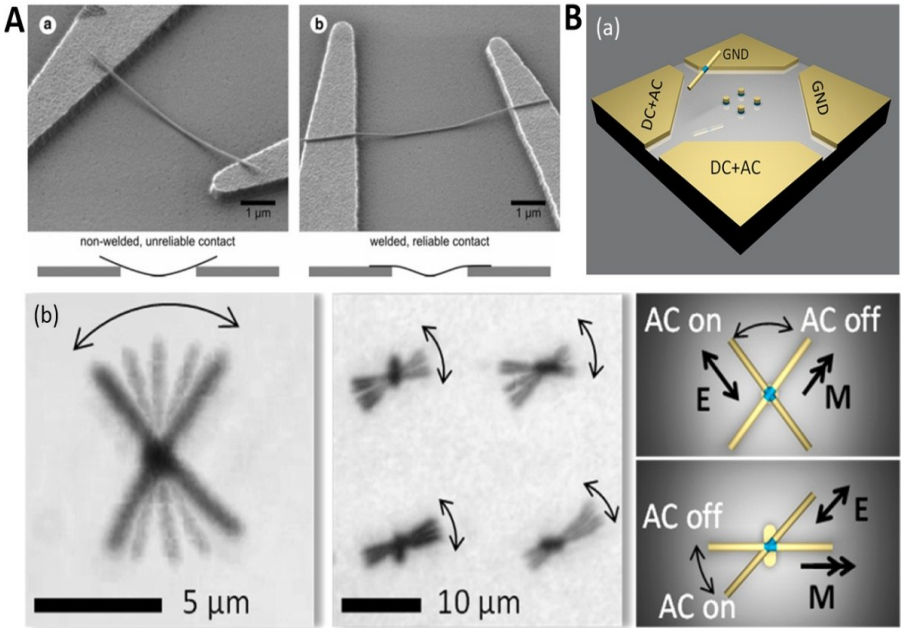

Fig. 5 Accurate DEP manipulation of single nanowire. (A): SEM image of DEP trapped SiNW. (a) Trapped SiNW without welding having insufficient contact to the electrodes. (b) SiNW welded to the electrodes with short pulse of higher voltage is closely clinging on the electrodes, which provides reliable contacts for electrical measurements. (B): (a) Schematic diagram of dielectrophoresis (DEP)-based setup consists of Au quadrupole electrodes with a magnetic nanoanchor array at the center. (b) Overlapped snapshots and schematic diagrams of oscillating nanowires assembled on a single disk magnetic nanoanchor and a 2x2 array of bar-shaped magnetic anchors.

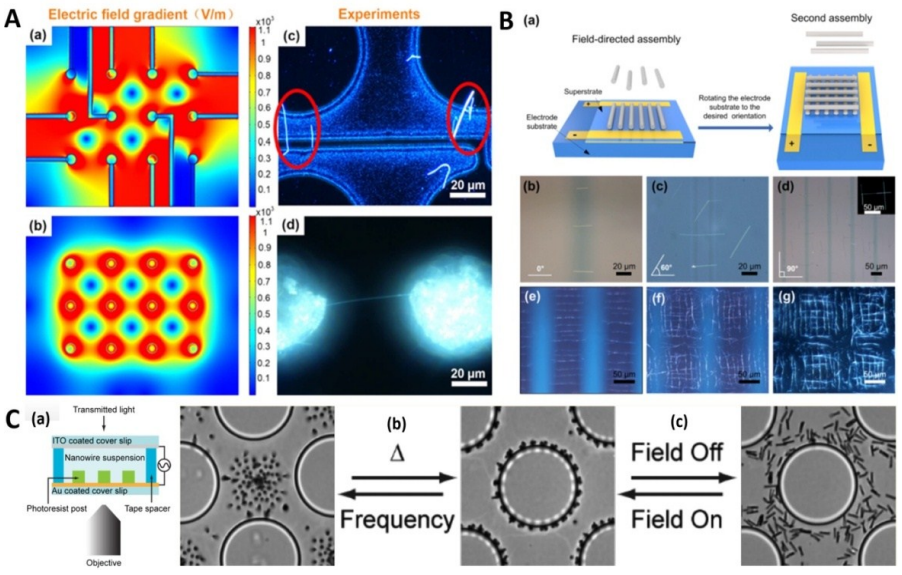

Fig. 6 Flexible DEP manipulation of nanomaterials. (A)**:** (a), (b) Contour plots of the electric field gradient of the dot matrix electrodes with and without lead. (c) The interference of the lead in the electric field distribution. (d) Dark-field image

This article is protected by copyright. All rights reserved.

illustrating that a nanowire hovers centered above two energized dot electrodes without interference from the lead. (B): (a) Schematic illustration of the multi-step nanowire assembly process. (b-g) Flexible assembly of Ag nanowire arrays with arbitrarily angle on an independent, removable PET film by rotating the reusable ITO electrodes. (C): (a) Side view schematic of experimental set up. (b) Nanowire assemblies could be reconfigured by changing the applied frequency. (c) When the field was off, nanowires laid parallel to the substrate. When the field was turned on, the nanowires stood perpendicular to the substrate.

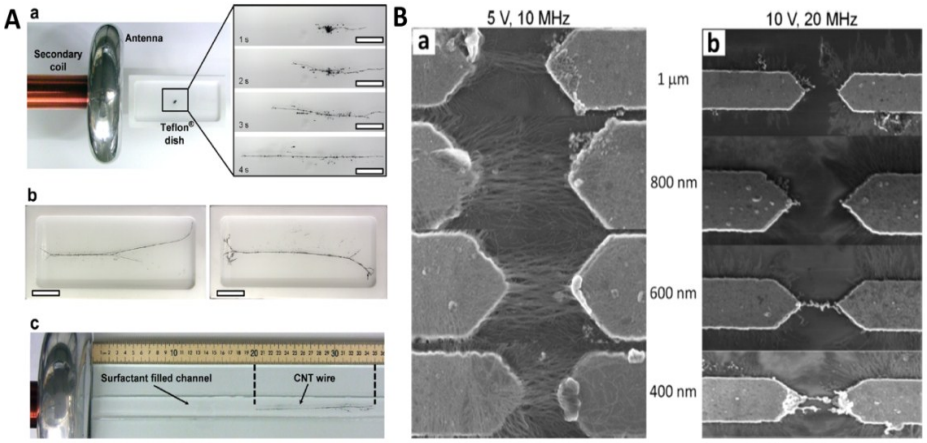

Fig. 7 Large scale DEP manipulation of nanomaterials. (A)： Teslaphoretic (TEP) directed self-assembly of bulk CNTs into long macroscale wires. (a) TEP system with a Teflon dish containing ~1 mg of CNT powder in a pool of 1% Pluronic water. (b) Directional control of nanotube wire growth using an electrically grounded metal plate located 10 cm away from the upper right corner and lower right corner of the Teflon dish. Scale bars = 3 cm. (c) Nanotube wire remotely self-assembled 30 cm away from the antenna in < 40 s. (B): Directed assembly of ultrathin Au Nanowires over large area by DEP. SEM images of nanowires aligned (a) between electrodes and (b) along the sides.

This article is protected by copyright. All rights reserved.

Accepted Article

Accepted Article

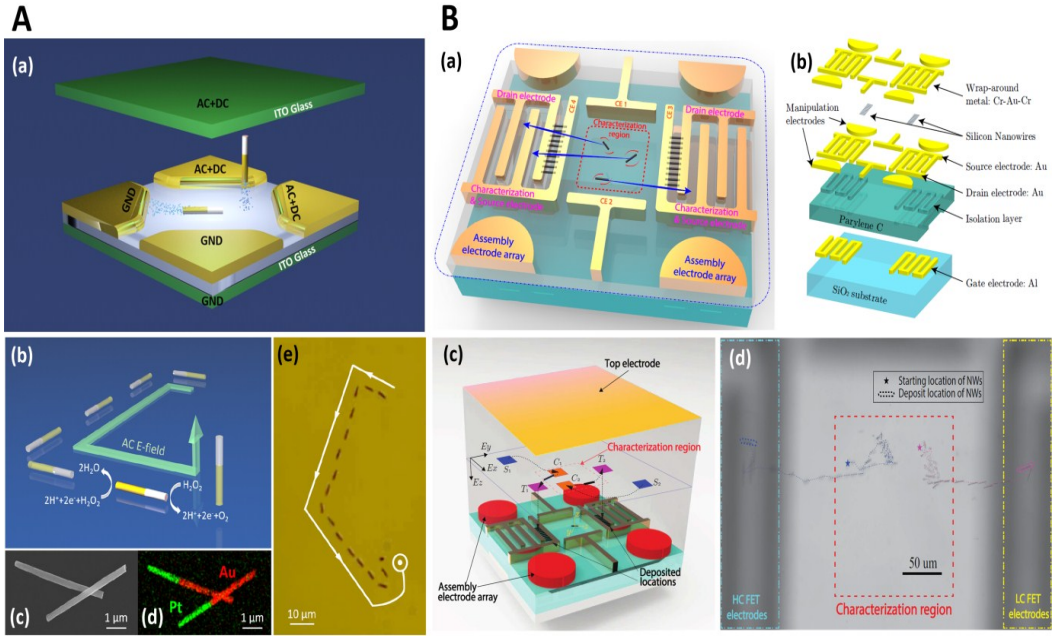

Fig. 8 Outstanding performance in the comprehensive ability of the three indicators (accuracy, flexibility, scale) in DEP manipulation of nanomaterials. (A): (a) Scheme of 3D orthogonal microelectrode setup. (b) Schematic diagram of 3D manipulations of Pt-Au catalytic nanomotors in H_2O_2 fuel with AC E-fields. (c) SEM and (d) energy-dispersive X-ray spectroscopy (EDX) images of Pt-Au catalytic nanomotors. (e) Overlapped snapshots of a catalytic nanomotor guided by AC E-fields. (B): (a) Schematic of the ACMAN system to fabricate nanowire-based FETs with selected electric properties. (b) Fabrication schematic for the Si NW-based bottom-gate FETs. (c) Schematic of microfluidic device with 2x2 independently actuated assembly electrode array on a bottom substrate, with a common top electrode. (d) Overlaid trajectories of two Si NWs separated by their different electrical conductivities using the ACMAN process.

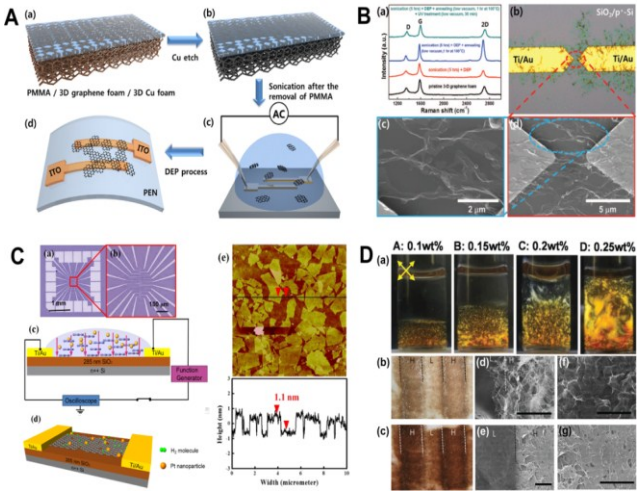

This article is protected by copyright. All rights reserved.

Accepted Article

Fig. 9 (A): Schematic of device fabrication process. (B): (a) Raman spectra after various treatments (b) microscope and (c, d) SEM images after DEP process. (C): (a) Optical microscopy image and (b) higher magnification optical microscopy image of the prepatterned parallel finger electrodes. (c) Schematic of the experimental setup for DEP processing. (d) Schematic showing assembled GO nanostructures and Pt nanoparticles. (e) AFM image and height profile of GO nanostructures. (D): (a) Gravity-induced phase separation in bottles containing various concentrations of GO. (b) Optical reflective and (c) transmissive microscopic images of 0.25 wt% GO freeze-dried fracture sample. (d-g) SEM image of GO freeze-dried fracture sample near the boundary of the H and L regions. Scale bars, 100 μm.

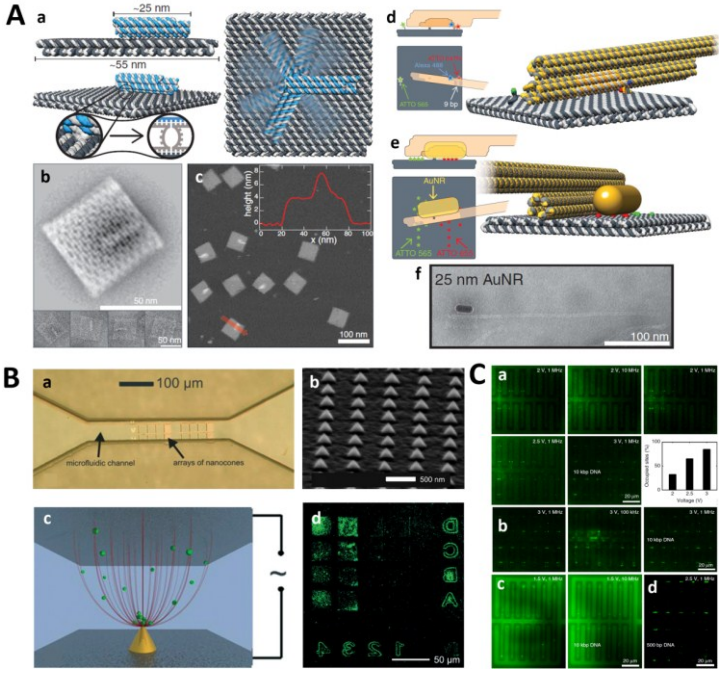

Fig. 10 (A): A molecular platform with an integrated rotatable positioning arm. (a) Sketch of the DNA origami structure in side and top view. (b) TEM class-average and single-particle micrographs of the structure. (c) AFM image of particles on mica. (d-e) Electrically controlled movement of molecules and nanoparticles. (f) TEM micrograph of a structure with a 25-nm AuNR. (B): (a) Top view of arrays of gold nanocones in a microfluidic channel. (b) SEM images of arrays of gold nanocones. (c) Schematic of the capture of particles by a metallic nanocone via dielectrophoresis. (d) Fluorescence image of BSA molecules arrays captured by DEP. (C): (a-d) DEP manipulation of DNA molecules.

This article is protected by copyright. All rights reserved.